inorganics

MDPI

Article

Two Perovskite Modifications of $BiFe_{0.6}Mn_{0.4}O_3$ Prepared by High-Pressure and Post-Synthesis Annealing at Ambient Pressure

Alexei A. Belik

Research Center for Materials Nanoarchitectonics (MANA), National Institute for Materials Science (NIMS), Namiki 1-1, Tsukuba 305-0044, Ibaraki, Japan; alexei.belik@nims.go.jp

Abstract: $BiFeO_3$-related perovskite-type materials attract a lot of attention from the viewpoint of applications and fundamental science. In this work, we prepared two modifications of heavily Mn-doped $BiFeO_3$ with the composition of $BiFe_{0.6}Mn_{0.4}O_3$. A high-pressure (HP) modification was prepared at about 6 GPa and 1400 K. An ambient pressure (AP) modification was prepared by heating the HP modification at 780 K in the air at AP (post-synthesis annealing). Crystal structures of both modifications and in situ transformation were investigated with synchrotron powder X-ray diffraction. The transformation started at about 700 K and finished at about 780 K. The HP modification crystallized in space group *Pnma* with a = 5.57956 Å, b = 15.70576 Å, and c = 11.22557 Å, and the AP modification crystallized in space group *Pbam* with a = 5.63839 Å, b = 11.2710 Å, and c = 7.75923 Å (all parameters were at room temperature). Post-synthesis annealing of the HP modification (conversion polymorphism) is the only way to prepare the *Pbam* modification of oxygen stoichiometric $BiFe_{0.6}Mn_{0.4}O_3$. Magnetic properties of both modifications have been reported. The Néel temperatures are T_N = 350 K (HP) and T_N = 335 K (AP). HP modification shows larger spin canting. Both modifications show negative magnetization phenomena at low temperatures in low magnetic fields.

Keywords: multiferroics; doped $BiFeO_3$; high-pressure synthesis; irreversible transformations; conversion polymorphism

Citation: Belik, A.A. Two Perovskite Modifications of $BiFe_{0.6}Mn_{0.4}O_3$ Prepared by High-Pressure and Post-Synthesis Annealing at Ambient Pressure. *Inorganics* **2024**, *12*, 226. https://doi.org/10.3390/inorganics12080226

Academic Editors: Shuang Liang and Mingyue Zhang

Received: 29 July 2024
Revised: 16 August 2024
Accepted: 16 August 2024
Published: 19 August 2024

1. Introduction

Materials with all possible ordered magnetic spins and electric dipoles are called multiferroics nowadays [1–4], even though the term 'multiferroics' was initially introduced only for materials with simultaneous ferroelectric and ferromagnetic (FM) orders [5]. The $BiFeO_3$ perovskite is arguably the most studied multiferroic material [6], which attracted renewed interest after the work on thin-film samples [7]. $BiFeO_3$ belongs to the so-called type-I multiferroics [1–4]. In type-I multiferroics, a ferroelectric transition takes place at a different temperature in comparison with the temperature of a magnetic transition because magnetism and ferroelectricity have different origins. In $BiFeO_3$, the ferroelectric (FE) transition takes place at T_{FE} = 1100 K and originates from the activity of a lone-electron pair of Bi^{3+} cations [6]. $BiFeO_3$ crystallizes in the space group $R3c$ below T_{FE}. The pure antiferromagnetic (AFM) transition occurs at the Néel temperature T_N = 643 K and originates from superexchange interactions between magnetic Fe^{3+} cations [6]. Magnetic Fe^{3+} cations on the three-dimensional perovskite lattice usually give large magnetic transition temperatures above room temperature, as in $RFeO_3$ [8]. Neighboring spins are canted in $BiFeO_3$. However, the absence of any net FM moments in $BiFeO_3$ originates from a long period of incommensurate spin ordering, which averages the total net moment to zero [6].

Different crystallographic phases have close energies and compete with each other in $BiFeO_3$, as can be seen from a cascade of structural phase transitions under high pressure [9–11] and the stabilization of different phases with small amounts of doping on

both Bi and Fe sublattices [12–17]. At ambient pressure (AP), solid solutions can usually be prepared in whole compositional ranges from $x = 0$ to $x = 1$ in cases of (1) isovalent doping in the Bi sublattice, for example, $Bi_{1-x}R_xFeO_3$ with R^{3+} = rare-earth elements [13–15] and (2) simultaneous aliovalent doping at both Bi and Fe sublattices, for example, $(1-x)BiFeO_{3-x}PbTiO_3$ [18] and $(1-x)BiFeO_{3-x}BaTiO_3$ [19]. On the other hand, doping only at the Fe sublattice, $BiFe_{1-x}M_xO_3$ with M = 3*d* transition metals can be realized in very limited compositional ranges at AP. A maximum doping level of about $x = 0.3$ is realized in the $BiFe_{1-x}Mn_xO_3$ system at AP [17,20,21]. The main reason for this seems to be the fact that $BiMO_3$ with other 3*d* transition metals (except for M = Fe) is not stable at AP [22].

During two decades of intensive research on $BiFeO_3$-related materials, different preparation methods of $Bi_{1-x}R_xFeO_3$ and $BiFe_{1-x}M_xO_3$ have been developed and used, for example, different modifications of a standard solid-state synthesis (e.g., rapid synthesis) in different atmospheres, high-pressure (HP) high-temperature methods, variable soft-chemistry methods, plasma syntheses, and so on. However, in the case of $BiFe_{1-x}Mn_xO_3$ solid solutions, only standard solid-state synthesis in different atmospheres and HP high-temperature methods have been described in the literature.

The HP high-temperature method has significant advantages because $BiFe_{1-x}M_xO_3$ solid solutions for compositional ranges from $x = 0$ to $x = 1$ can be prepared [17,23–25]. This method also often gives different modifications of $BiFe_{1-x}M_xO_3$ in comparison with AP synthesis. In addition, a "conversion polymorphism" phenomenon [23] is sometimes observed in HP phases of $BiFe_{1-x}M_xO_3$ when post-synthesis annealing produces new phases of $BiFe_{1-x}M_xO_3$, which cannot be accessible using other methods.

In this work, we describe such a "conversion polymorphism" phenomenon in the high-pressure-synthesized $BiFe_{0.6}Mn_{0.4}O_3$. An HP modification was prepared at about 6 GPa and 1500 K. An AP modification was prepared by heating the HP modification at 773 K in air at AP. The HP modification crystallizes in the space group *Pnma* and is isostructural with some $Bi_{1-x}R_xFeO_3$ compounds, while the AP modification crystallizes in the space group *Pbam* and is isostructural with an antiferroelectic phase of $PbZrO_3$. The magnetic properties of both modifications were studied.

2. Results and Discussion

The as-synthesized HP-$BiFe_{0.6}Mn_{0.4}O_3$, crystallized in a complex $PbZrO_3$-related superstructure $\sqrt{2}a_p \times 4a_p \times 2\sqrt{2}a_p$ (where a_p (≈3.95 Å) is the parameter of the cubic perovskite subcell) with $a = 5.57956(3)$ Å, $b = 15.70576(8)$ Å, $c = 11.22557(6)$ Å, and the space group *Pnma* (No. 62) [17]. HP-$BiFe_{0.6}Mn_{0.4}O_3$ contained a small amount of $Bi_2O_2CO_3$ impurity (about 1.1 weight%). HP-$BiFe_{0.6}Mn_{0.4}O_3$ with heavy doping at the Fe sublattice has the same (super)structure as $Bi_{0.82}La_{0.18}FeO_3$ [13] and $Bi_{0.85}Nd_{0.15}FeO_3$ [26] with small doping at the Bi sublattice. This fact shows that the centrosymmetric *Pnma* structure with $\sqrt{2}a_p \times 4a_p \times 2\sqrt{2}a_p$ is one of the competing phases with the ferroelectric *R3c* structure of the parent $BiFeO_3$. Refined structural parameters of HP-$BiFe_{0.6}Mn_{0.4}O_3$ are summarized in Table 1, and Figure 1a shows fragments of experimental, calculated, and difference synchrotron XRPD data after the Rietveld fit.

In situ high-temperature structural studies of HP-$BiFe_{0.6}Mn_{0.4}O_3$ showed that synchrotron patterns (and superstructure reflections) did not change from 297 K to 680 K (Figure 2). However, the temperature dependence of the lattice parameters of HP-$BiFe_{0.6}Mn_{0.4}O_3$ showed some anomalies above 620 K (Figure 3). At 700 K, new reflections started to emerge (Figure 2). With further increases in temperature, intensities of new reflections increased, while intensities of superstructure reflections corresponding to the *Pnma* model ($\sqrt{2}a_p \times 4a_p \times 2\sqrt{2}a_p$) decreased. Finally, at 780 K, all superstructure reflections corresponding to the *Pnma* model disappeared (Figure 2). All peaks at 780 K could be indexed in a $\sqrt{2}a_p \times 2\sqrt{2}a_p \times 2a_p$ superstructure with $a = 5.64743(13)$ Å, $b = 11.2983(2)$ Å, $c = 7.82606(5)$ Å, and the space group *Pbam* (No. 55). During cooling, the new modification remained down to 297 K; this modification can be called AP-$BiFe_{0.6}Mn_{0.4}O_3$. Refined structural parameters of AP-$BiFe_{0.6}Mn_{0.4}O_3$ at 297 K and 780 K

are summarized in Tables 2 and 3, and Figure 1b shows the fragments of experimental, calculated, and difference synchrotron XRPD data after the Rietveld fit at 297 K as an example. The temperature dependence of the lattice parameters on heating and cooling is illustrated in Figures 3 and 4. The crystal structure of AP-$BiFe_{0.6}Mn_{0.4}O_3$ is isostructural with the antiferroelectric phase of $PbZrO_3$ [27,28]. This crystal structure was also reported, for example, for $Bi_{0.8}La_{0.2}FeO_3$ [11], $Bi_{0.875}Pr_{0.125}FeO_3$ [15], and $Bi_{0.89}Ca_{0.11}FeO_3$ [16]. Therefore, this centrosymmetric *Pbam* structure with $\sqrt{2}a_p \times 2\sqrt{2}a_p \times 2a_p$ is another competing phase.

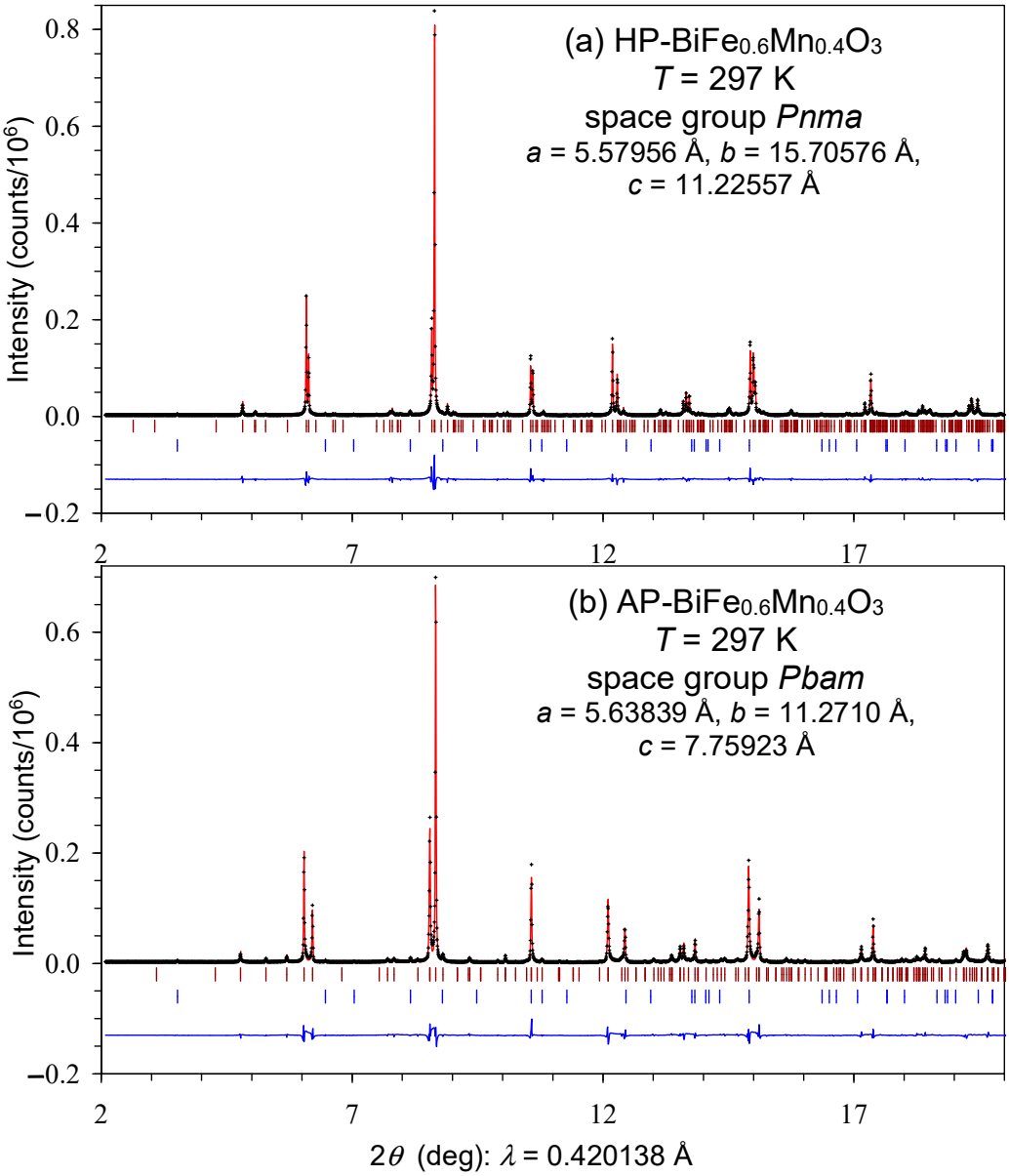

Figure 1. The experimental (black crosses), calculated (red line), and difference (blue line at the bottom) synchrotron powder X-ray diffraction patterns of (**a**) HP-$BiFe_{0.6}Mn_{0.4}O_3$ and (**b**) AP-$BiFe_{0.6}Mn_{0.4}O_3$ at T = 297 K between 2° and 20°. The tick marks show possible Bragg reflection positions for the main phase (brown) and $Bi_2O_2CO_3$ impurity (blue) from top to bottom.

Table 1. Structure parameters of HP-$BiFe_{0.6}Mn_{0.4}O_3$ at 297 K refined from synchrotron XRPD data.

Atom	WP	*x*/*a*	*y*/*b*	*z*/*c*	B_{iso} (Å^2)
Bi1	8*d*	0.2169(5)	0.00935(9)	0.62476(16)	1.18(5)
Bi2	4*c*	0.2135(7)	0.25	0.6251(2)	1.37(7)
Bi3	4*c*	0.7729(7)	0.25	0.3635(2)	1.55(7)
FeMn1	8*d*	0.2397(12)	0.1227(6)	0.8779(7)	1.06(11)
FeMn2	8*d*	0.2615(11)	0.6249(5)	0.8770(6)	0.54(10)
O1	8*d*	0.809(4)	−0.0026(12)	0.6556(18)	0.24(16)
O2	4*c*	0.641(6)	0.25	0.653(3)	=*B*(O1)
O3	4*c*	0.177(7)	0.25	0.425(3)	=*B*(O1)
O4	8*d*	0.099(4)	0.1267(17)	0.7217(19)	=*B*(O1)
O5	8*d*	−0.003(4)	0.3942(15)	−0.0260(21)	=*B*(O1)
O6	8*d*	0.041(4)	0.6458(14)	0.7424(23)	=*B*(O1)
O7	8*d*	0.019(5)	0.3989(13)	0.516(3)	=*B*(O1)

Source: Synchrotron powder X-ray diffraction (λ = 0.42014 Å); *d*-space range used in the refinement: 0.420–11.563 Å. Crystal system: orthorhombic; space group *Pnma* (No 62); *Z* = 16. Molecular weight: 312.458 g/mol. The occupation factors, *g*, of all Bi and O sites, are unity; *g* = 0.6Fe + 0.4Mn for FeMn1 and FeMn2. WP: Wyckoff position. Impurity: $Bi_2O_2CO_3$ (1.1 wt.%). *a* = 5.57956(3) Å, *b* =15.70576(8) Å, *c* = 11.22557(6) Å, and *V* = 983.711 (9) Å^3; R_{wp} = 9.02%, R_p = 6.43%, R_B = 5.14%, and R_F = 6.78%; ρ_{cal} = 8.439 g/cm^3.

Table 2. Structure parameters of AP-$BiFe_{0.6}Mn_{0.4}O_3$ at 297 K refined from synchrotron XRPD data.

Atom	WP	*x*/*a*	*y*/*b*	*z*/*c*	B_{iso} (Å^2)
Bi1	4*g*	0.2431(3)	0.3807(3)	0	2.15(6)
Bi2	4*h*	0.2061(3)	0.3676(2)	0.5	0.32(3)
FeMn	8*i*	0.2552(6)	0.1239(14)	0.2487(13)	0.80(5)
O1	4*g*	0.241(4)	0.162(3)	0	1.8(9)
O2	4*h*	0.338(5)	0.093(3)	0.5	1.2(7)
O3	8*i*	0.078(4)	0.2649(16)	0.275(3)	1.7(5)
O4	4*f*	0	0.5	0.188(3)	1.3(7)
O5	4*e*	0	0	0.202(4)	2.4(8)

Source: Synchrotron powder X-ray diffraction (λ = 0.42014 Å); *d*-space range used in the refinement: 0.420–11.563 Å. Crystal system: orthorhombic; space group *Pbam* (No. 55); *Z* = 8. Molecular weight: 312.458 g/mol. The occupation factors, *g*, of all Bi and O sites, are unity; *g* = 0.6Fe + 0.4Mn for FeMn. WP: Wyckoff position. Impurity: $Bi_2O_2CO_3$ (1.1 wt.%). *a* = 5.63839(12) Å, *b* = 11.2710(2) Å, *c* = 7.75923(8) Å, and *V* = 493.103(15) Å^3; R_{wp} = 11.93%, R_p = 8.40%, R_B = 4.92%, and R_F = 2.66%; ρ_{cal} = 8.418 g/cm^3.

Table 3. Structure parameters of AP-$BiFe_{0.6}Mn_{0.4}O_3$ at 780 K refined from synchrotron XRPD data.

Atom	WP	*x*/*a*	*y*/*b*	*z*/*c*	B_{iso} (Å^2)
Bi1	4*g*	0.2383(4)	0.3786(5)	0	3.31(13)
Bi2	4*h*	0.2141(5)	0.3700(4)	0.5	1.91(9)
FeMn	8*i*	0.2524(9)	0.1246(25)	0.2499(17)	1.56(6)
O1	4*g*	0.257(5)	0.170(5)	0	2.3 (3)
O2	4*h*	0.304(6)	0.091(5)	0.5	=*B*(O1)
O3	8*i*	0.075(4)	0.2678(19)	0.271(4)	=*B*(O1)
O4	4*f*	0	0.5	0.185(4)	=*B*(O1)
O5	4*e*	0	0	0.206(4)	=*B*(O1)

Source: Synchrotron powder X-ray diffraction (λ = 0.42014 Å); *d*-space range used in the refinement: 0.549–11.563 Å. Crystal system: orthorhombic; space group *Pbam* (No. 55); *Z* = 8. Molecular weight: 312.458 g/mol. The occupation factors, *g*, of all Bi and O sites, are unity; *g* = 0.6Fe + 0.4Mn for FeMn. WP: Wyckoff position. Impurity: $Bi_2O_2CO_3$ (1.1 wt.%). *a* = 5.64743(13) Å, *b* = 11.2983(2) Å, *c* = 7.82606(5) Å, and *V* = 499.353(16) Å^3; R_{wp} = 10.94%, R_p = 7.43%, R_B = 5.81%, and R_F = 4.97%; ρ_{cal} = 8.312 g/cm^3.

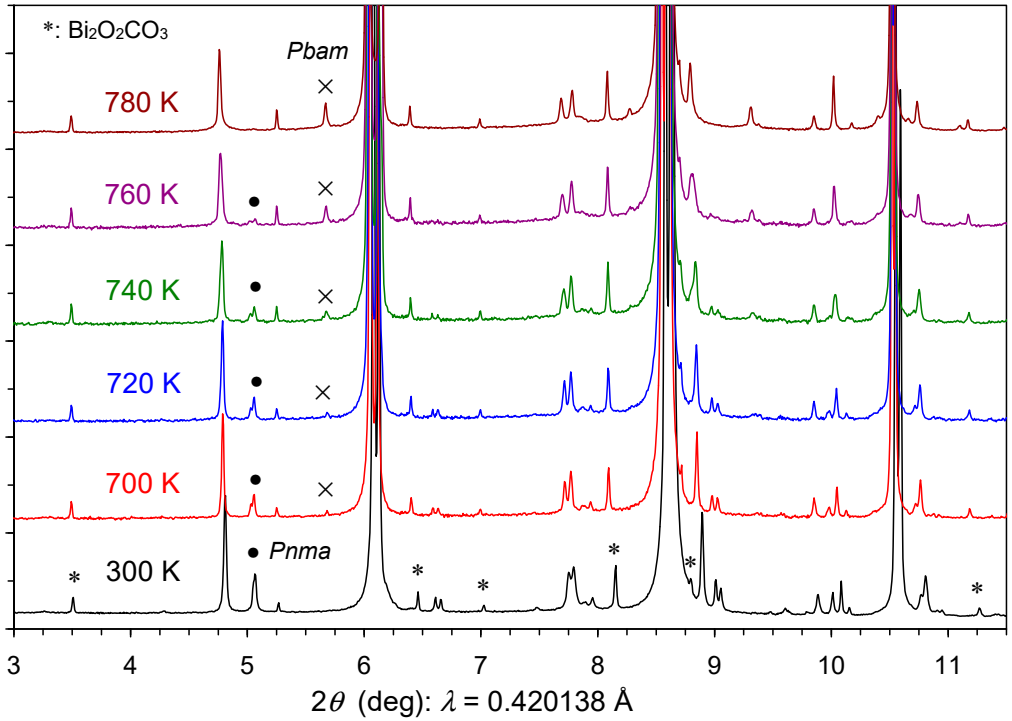

Figure 2. Temperature evolution of synchrotron powder X-ray diffraction patterns of HP-$BiFe_{0.6}Mn_{0.4}O_3$ at selected temperatures. The zoomed parts emphasizing superstructure reflections are shown. Stars mark reflections from $Bi_2O_2CO_3$ impurity. Black circles show characteristic reflections from HP-$BiFe_{0.6}Mn_{0.4}O_3$, and crosses show a characteristic reflection from AP-$BiFe_{0.6}Mn_{0.4}O_3$.

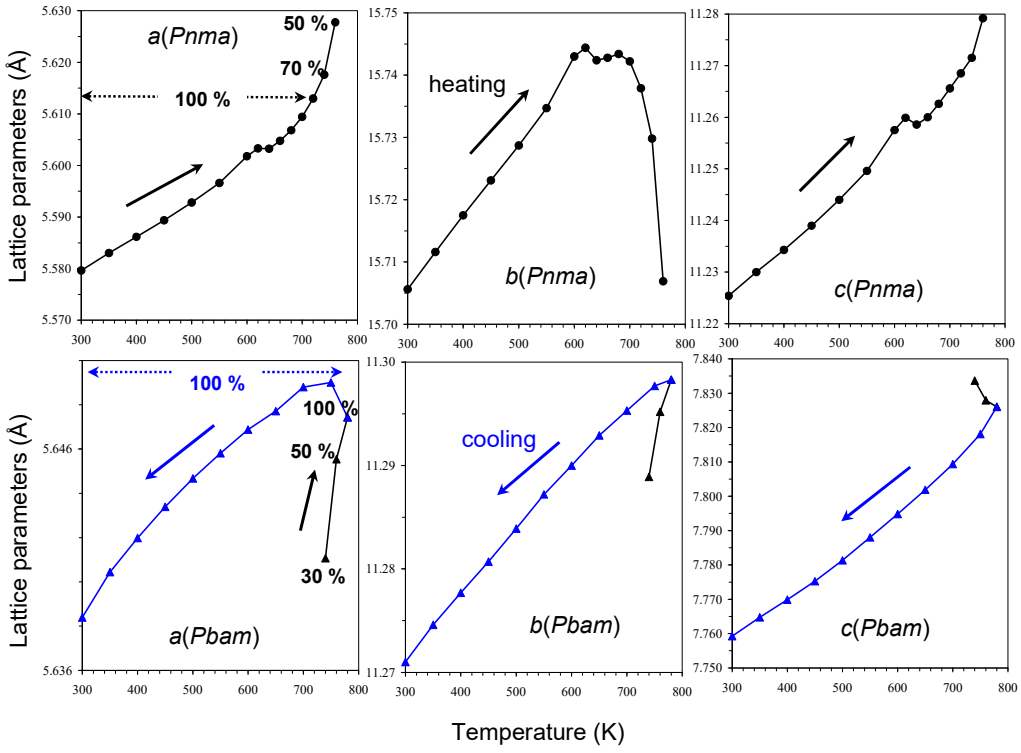

Figure 3. (**Up**) Temperature dependence of the lattice parameters of HP-$BiFe_{0.6}Mn_{0.4}O_3$ on heating. (**Down**) Temperature dependence of the lattice parameters of AP-$BiFe_{0.6}Mn_{0.4}O_3$ on heating (black symbols) and cooling (blue symbols). Numbers show weight fractions (in%) of the corresponding phases.

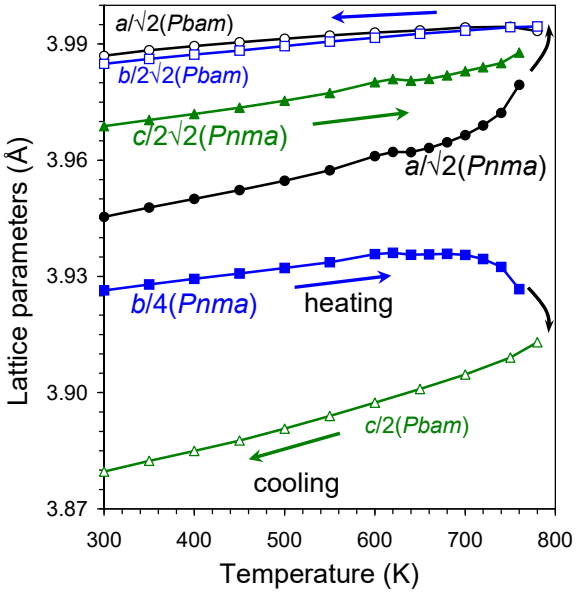

Figure 4. Temperature dependence of the normalized lattice parameters of HP-$BiFe_{0.6}Mn_{0.4}O_3$ (*Pnma*) on heating and AP-$BiFe_{0.6}Mn_{0.4}O_3$ (*Pbam*) on cooling.

We note that the *Pnma* model with the $\sqrt{2}a_p \times 4a_p \times 2\sqrt{2}a_p$ superstructure is a direct subgroup of the *Pbam* model with the $\sqrt{2}a_p \times 2\sqrt{2}a_p \times 2a_p$ superstructure. In many cases, additional superstructure reflections of the *Pnma* model are very weak. Therefore, a real *Pnma* model was sometimes replaced by a simplified *Pbam* model to obtain reliable, refined structural parameters [29], as the *Pnma* model has 32 refined fractional coordinates of atoms, while the *Pbam* model has 16 such parameters. However, in the case of $BiFe_{0.6}Mn_{0.4}O_3$, the two modifications were quite different as the fundamental perovskite lattice parameters (a_p) were different (Figure 4), and the reflection splitting of strong fundamental reflections was different at room temperature (Figures 1 and 5). Therefore, the AP-$BiFe_{0.6}Mn_{0.4}O_3$ modification could not be considered as a simplified version of the HP-$BiFe_{0.6}Mn_{0.4}O_3$ modification.

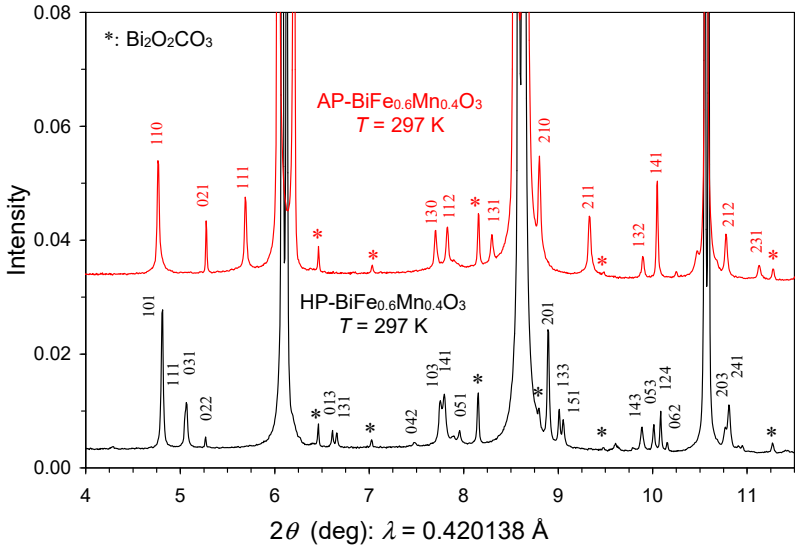

Figure 5. Zoomed parts (to emphasize superstructure reflections) of room-temperature synchrotron powder X-ray diffraction patterns of HP-$BiFe_{0.6}Mn_{0.4}O_3$ and AP-$BiFe_{0.6}Mn_{0.4}O_3$. Stars mark reflections from $Bi_2O_2CO_3$ impurity. The (*hkl*) indexes of main superstructure reflections are given. Intensities were normalized to 1, and data for the AP modification were shifted by +0.03 (or 3%).

Figure 6 shows the crystal structures of HP-$BiFe_{0.6}Mn_{0.4}O_3$, AP-$BiFe_{0.6}Mn_{0.4}O_3$, and $PbZrO_3$ (at room temperature) for comparison [28]. $(FeMn)O_6$ octahedra are strongly distorted in both modifications; a similar effect is observed for TiO_6 octahedra in $PbZrO_3$. These features can be explained by the formation of strong covalent Bi–O and Pb–O bonds originating from the stereochemical activity of the lone pair of Bi^{3+} and Pb^{2+} cations. In other words, elongated (FeMn)–O or Zr–O bonds are simultaneously involved in short Bi–O or Pb–O bonds, respectively [17]. The HP synthesis method usually stabilizes a modification with higher density. The density of HP-$BiFe_{0.6}Mn_{0.4}O_3$ (8.439 g/cm^3) was indeed slightly higher than that of AP-$BiFe_{0.6}Mn_{0.4}O_3$ (8.418 g/cm^3) (Tables 1 and 2). To achieve higher density and to accommodate the lone pair of Bi^{3+}, an additional octahedral rotation along the *b* axis was necessary (Figure 6c), resulting in a superstructure and a stressed structure in HP-$BiFe_{0.6}Mn_{0.4}O_3$. Heating at AP results in the release of stress. The transformation of HP-$BiFe_{0.6}Mn_{0.4}O_3$ into AP-$BiFe_{0.6}Mn_{0.4}O_3$ involves small rotations of $(FeMn)O_6$ octahedra (Figure 6b,c) and small shifts of Bi^{3+} cations.

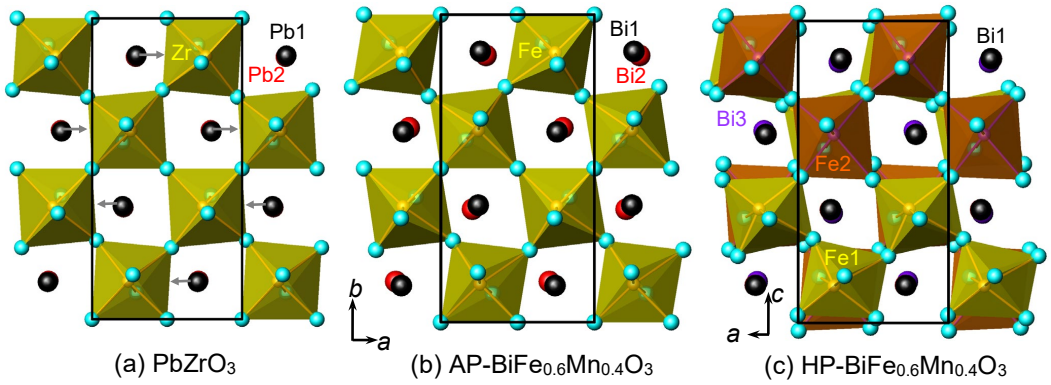

Figure 6. Fragments of crystal structures of (**a**) $PbZrO_3$ (at room temperature [28]), (**b**) AP-$BiFe_{0.6}Mn_{0.4}O_3$, and (**c**) HP-$BiFe_{0.6}Mn_{0.4}O_3$ (Bi2 atoms are hidden by Bi1 and Bi3). Arrows in panel (**a**) show the displacements of Pb^{2+} inside cavities. For simplicity, octahedral sites are marked as Fe, Fe1, and Fe2.

No clear DSC anomalies were observed during the first round of heating of HP-$BiFe_{0.6}Mn_{0.4}O_3$, suggesting that the thermal effect of the HP-to-AP transformation was very weak. The absence of any DSC anomalies could also be related to the fact that the HP-to-AP transformation occurred in a wide temperature range from 700 K to 780 K (Figure 2), preventing any detectable thermal effect. No clear DSC anomalies were observed during the first cooling of the already-formed AP-$BiFe_{0.6}Mn_{0.4}O_3$, and no DSC anomalies were detected during the second DSC run on the already-formed AP-$BiFe_{0.6}Mn_{0.4}O_3$. This fact suggests that AP-$BiFe_{0.6}Mn_{0.4}O_3$ did not undergo any structural phase transitions between 297 K and 773 K. In the case of $BiFe_{0.6}Mn_{0.4}O_3$, we observed a full transformation of an HP structure into another AP structure. In other members of HP-$BiFe_{1-x}Mn_xO_3$ solid solutions, partial transformations into different modifications were reported [30,31].

Temperature-dependent magnetic measurements showed that the Néel temperatures were T_N = 350 K for HP-$BiFe_{0.6}Mn_{0.4}O_3$ and T_N = 335 K for AP-$BiFe_{0.6}Mn_{0.4}O_3$ (Figures 7 and 8). *M* versus *H* measurements showed that HP-$BiFe_{0.6}Mn_{0.4}O_3$ had larger spin canting, especially at *T* = 5 K, as a clear hysteresis opened up (Figures 9 and 10). At *T* = 100, 200, and 300 K, the *M* versus *H* curves of HP-$BiFe_{0.6}Mn_{0.4}O_3$ were nearly linear with narrow cigar-type hysteresis, suggesting that spin canting was quite small. At *T* = 5, 100, 200, and 300 K, the *M* versus *H* curves of AP-$BiFe_{0.6}Mn_{0.4}O_3$ were almost linear, suggesting nearly complete AFM states. Above T_N, at *T* = 400 K, the *M* versus *H* curves of both modifications were linear because of the paramagnetic state (Figure 11) and coincided with each other; in other words, the *M* versus *H* curves were independent of the crystal structure. Exchange-bias-like effects were observed on the *M* versus *H* curves: at *T* = 5 K (negative exchange-bias-like effect) in AP-$BiFe_{0.6}Mn_{0.4}O_3$ and at *T* = 100 K (positive exchange-bias-like effect) and 200 K (negative exchange-bias-like effect) in HP-$BiFe_{0.6}Mn_{0.4}O_3$ (Figure 10).

Exchange-bias-like effects were observed in other $BiFeO_3$-based solid solutions [24,32,33]. In many cases, the "extrinsic" origins of exchange-bias-like effects were suggested, such as the presence of an antiferromagnetic core and a diluted antiferromagnetic shell [32] or non-uniform structure distortions and magnetic phase separation [33].

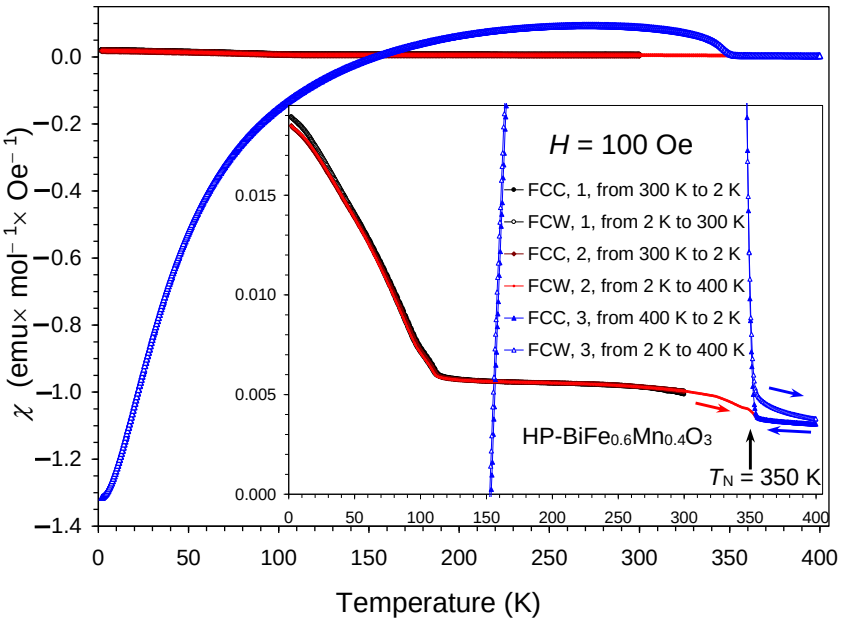

Figure 7. Magnetic properties of virgin HP-$BiFe_{0.6}Mn_{0.4}O_3$ (*Pnma*) (a pellet of 41.12 mg). Field-cooled on cooling (FCC) and field-cooled on warming (FCW) χ versus T curves at H = 100 Oe are shown. The first run was measured from 300 K to 2 K and from 2 K to 300 K. The second run was measured from 300 K to 2 K and from 2 K to 400 K. The third run was measured from 400 K to 2 K and from 2 K to 400 K. Insets show the zoomed parts. The magnetic field remained the same (unchanged) through all three runs.

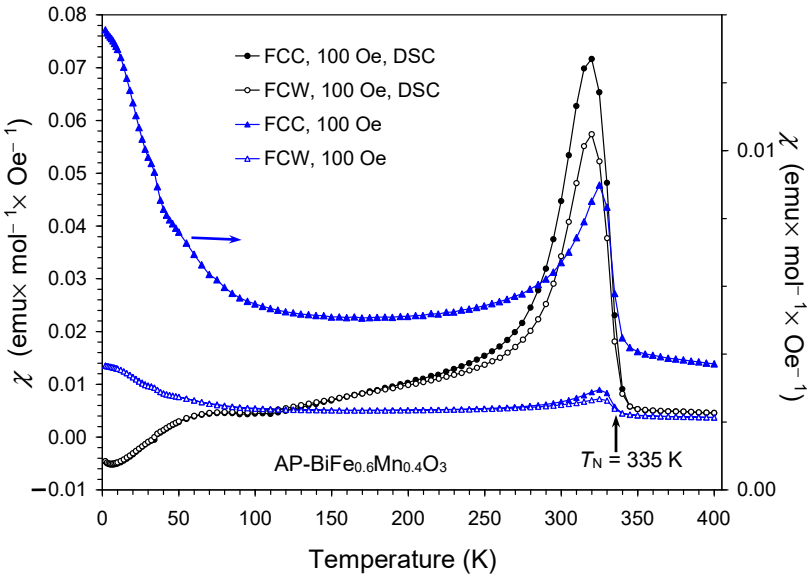

Figure 8. Magnetic properties of AP-$BiFe_{0.6}Mn_{0.4}O_3$ (*Pbam*). Field-cooled on cooling (FCC) and field-cooled on warming (FCW) χ versus T curves at H = 100 Oe are presented. The data for two samples are shown: an AP-$BiFe_{0.6}Mn_{0.4}O_3$ sample prepared in a furnace (a pellet of 41.12 mg) is shown by blue triangles; an AP-$BiFe_{0.6}Mn_{0.4}O_3$ sample prepared in a DSC experiment is shown by black circles (powder of 9.00 mg). The right-hand axis gives the same FCC curve for an AP-$BiFe_{0.6}Mn_{0.4}O_3$ sample prepared in a furnace.

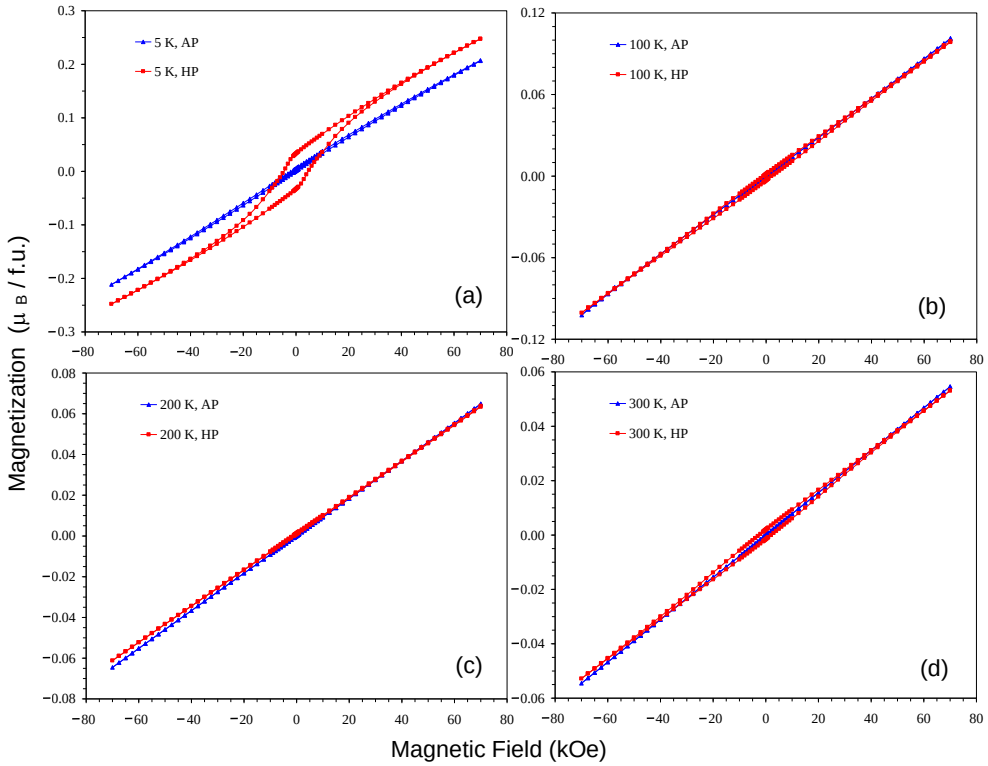

Figure 9. Comparison of magnetic properties of HP-$BiFe_{0.6}Mn_{0.4}O_3$ (*Pnma*) and AP-$BiFe_{0.6}Mn_{0.4}O_3$ (*Pbam*) (pellets of 41.12 mg): *M* versus *H* curves at (**a**) *T* = 5 K, (**b**) *T* = 100 K, (**c**) *T* = 200 K, and (**d**) *T* = 300 K.

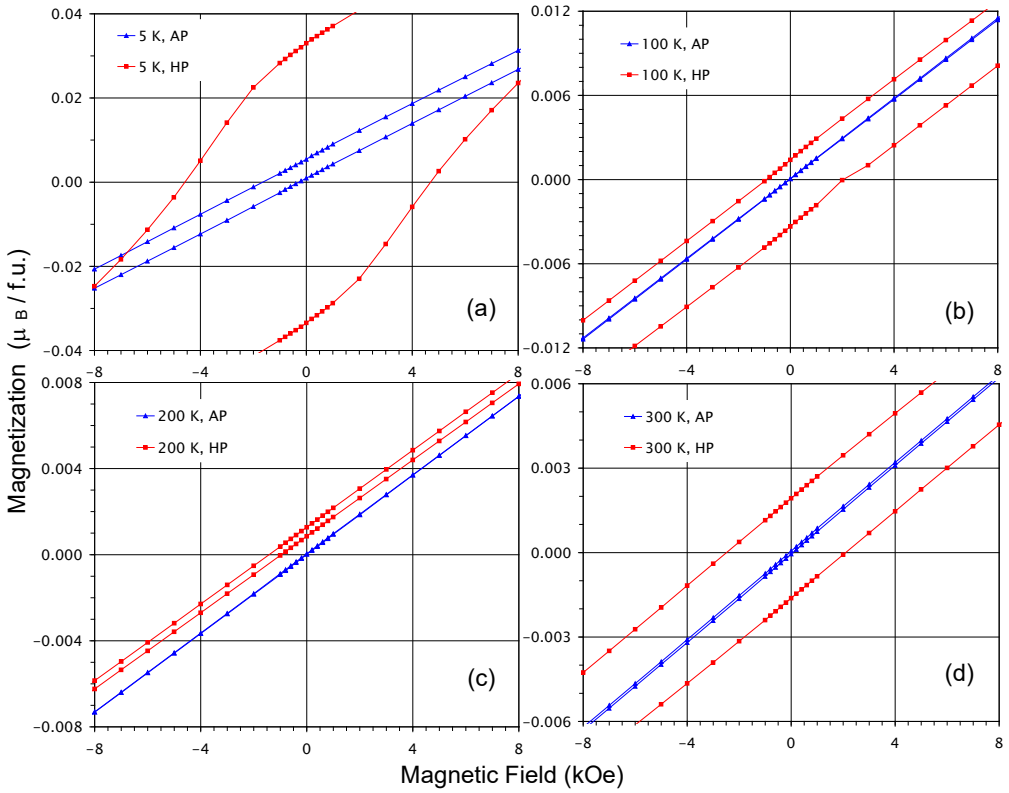

Figure 10. Comparison of magnetic properties of HP-$BiFe_{0.6}Mn_{0.4}O_3$ (*Pnma*) and AP-$BiFe_{0.6}Mn_{0.4}O_3$ (*Pbam*) (pellets of 41.12 mg): the zoomed parts of the *M* versus *H* curves are shown between −8 kOe and 8 kOe at (**a**) *T* = 5 K, (**b**) *T* = 100 K, (**c**) *T* = 200 K, and (**d**) *T* = 300 K.

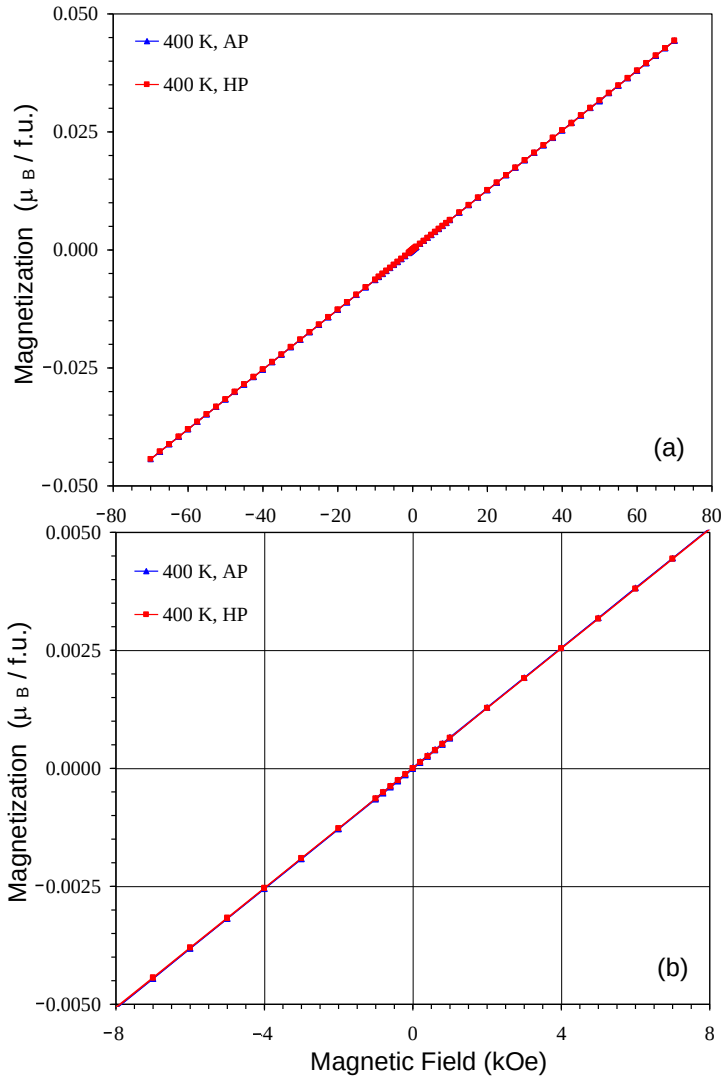

Figure 11. Comparison of magnetic properties of HP-$BiFe_{0.6}Mn_{0.4}O_3$ (*Pnma*) and AP-$BiFe_{0.6}Mn_{0.4}O_3$ (*Pbam*) (pellets of 41.12 mg): (**a**) *M* versus *H* curves between −70 kOe and 70 kOe at *T* = 400 K and (**b**) zoomed parts of the *M* versus *H* curves between −8 kOe and 8 kOe at *T* = 400 K.

HP-$BiFe_{0.6}Mn_{0.4}O_3$ showed peculiar magnetic susceptibility ($\chi = M/H$) curves at *H* = 100 Oe (Figure 7). When a virgin sample (meaning a sample taken directly after the synthesis; in other words, a sample that was not used for any magnetic measurements beforehand) was measured below its T_N (between 2 K and 300 K), the χ values were positive, and the FCC and FCW curves matched with each other and coincided on cycling. A sharp upturn was observed on the χ versus *T* curves below 120 K, suggesting the development of a weak FM moment in agreement with the *M* versus *H* curve at 5 K (Figure 9a). However, when the sample was heated above its T_N (up to 400 K), the χ values on the FCC and FCW curves were negative below 150 K, demonstrating a strong negative magnetization effect. Absolute *M* values (at *T* = 5 K) were about 70 times larger when measured from 400 K in comparison with the measurement from 300 K. It is probably for this reason that no anomalies were observed near 120 K when measurements were performed from 400 K because strong negative magnetization hid a weak upturn. In addition, the FCC and FCW curves of HP-$BiFe_{0.6}Mn_{0.4}O_3$ did not match above T_N as would be expected in a paramagnetic state, but their merging gradually took place on approaching 400 K. This observation could suggest that there are some ferromagnetic-like short-range correlations above T_N. On the other hand, the FCC and FCW curves of AP-$BiFe_{0.6}Mn_{0.4}O_3$ almost merged above T_N.

The magnetic properties of two AP-$BiFe_{0.6}Mn_{0.4}O_3$ samples are shown in Figure 8: one sample was obtained in a furnace; and another sample was obtained in a DSC experiment (see the experimental part). Both samples showed a magnetic transition at the same temperature of T_N = 335 K with different magnitudes of upturns below T_N. But, for both samples, the upturn below T_N was quite small, suggesting the development of small spin canting. The AP-$BiFe_{0.6}Mn_{0.4}O_3$ sample prepared in a DSC experiment showed a negative magnetization effect below 30 K. The absence of a negative magnetization effect in the AP-$BiFe_{0.6}Mn_{0.4}O_3$ sample prepared in a furnace suggests that this effect can be called "extrinsic" [24] when it is observed in some samples of AP-$BiFe_{0.6}Mn_{0.4}O_3$.

The introduction of Mn^{3+} cations into $BiFeO_3$ changes the crystal structure from a certain concentration of Mn^{3+} cations due to the existence of several competing structures and monotonically suppresses T_N from 643 K in $BiFeO_3$ to about 270 K in $BiFe_{0.5}Mn_{0.5}O_3$ [17,24,25]. The magnetic transition temperatures of $BiFe_{1-x}Mn_xO_3$ remain relatively high because of large concentrations of Fe^{3+} cations. Magnetic properties of $BiFeO_3$ [17] and AP-$BiFe_{0.6}Mn_{0.4}O_3$ were qualitatively similar in the sense that they both showed nearly pure AFM behavior despite their different crystal structures. The temperature dependence of magnetic susceptibility exhibited a sharp rise just below T_N in both compounds, indicating an initial development of uncompensated moments, but these uncompensated moments were suppressed at lower temperatures.

3. Materials and Methods

The HP modification of $BiFe_{0.6}Mn_{0.4}O_3$ was prepared from a stoichiometric mixture of Bi_2O_3 (Rare Metallic Co., Tokyo, Japan, 99.9999%), Fe_2O_3 (Rare Metallic Co., Tokyo, Japan, 99.999%), and Mn_2O_3. Single-phase Mn_2O_3 was prepared from a commercial MnO_2 chemical (Rare Metallic Co., Tokyo, Japan, 99.99%) by annealing in the air at 923 K for 24 h. The synthesis was performed at about 6 GPa and about 1400 K for 1.5 h in a sealed Au capsule using a belt-type HP instrument. After annealing at 1400 K, the sample was cooled down to room temperature by turning off the heating current, and the pressure was slowly released. As the used synthesis conditions for HP-$BiFe_{0.6}Mn_{0.4}O_3$ gave high-quality samples, we did not investigate the effects of synthesis conditions on the quality of HP-$BiFe_{0.6}Mn_{0.4}O_3$ and pressure–temperature stability ranges of HP-$BiFe_{0.6}Mn_{0.4}O_3$ (it was also out of the scope of the present work). But we did note that the pressure–temperature stability ranges of $BiFe_{1-x}Mn_xO_3$ solid solutions can be relatively large as a lower pressure of 5 GPa and lower temperature of 1073 K have been used in the literature [25]. The AP modification of $BiFe_{0.6}Mn_{0.4}O_3$ was prepared by heating HP-$BiFe_{0.6}Mn_{0.4}O_3$ in the air at AP at 773 K for 10 min (with a heating–cooling rate of 10 K/min).

X-ray powder diffraction (XRPD) data were collected at room temperature on a MiniFlex600 diffractometer (Rigaku, Tokyo, Japan) using CuKα radiation (2θ range of 8–100°, a step width of 0.02°, and a scan speed of 2°/min). Synchrotron XRPD data of HP-$BiFe_{0.6}Mn_{0.4}O_3$ were collected at 297 K upon heating to 780 K and cooling to 297 K using the beamline BL02B2 [34] of SPring-8, Japan. Intensity data were taken between 2.08° and 78.21° at a 0.006° interval in 2θ using a wavelength of λ = 0.420138 Å; however, data up to 60° (at 297 K) were used in the Rietveld analysis as no experimental reflections were observed above 60°. The measurement times were 300 s at 297 K and 780 K and 60 s for other temperatures. The sample was placed into an open Lindemann glass capillary tube (inner diameter: 0.1 mm), which was rotated during measurements. The Rietveld analysis of all XRPD data was performed using the *RIETAN-2000* program [35].

Magnetic measurements were performed on a SQUID magnetometer (Quantum Design MPMS3, San Diego, CA, USA) between 2 and 300 K (or 400 K) in an applied field of 100 Oe on cooling (FCC: field-cooled on cooling) and warming (FCW: field-cooled on warming). Isothermal magnetization measurements for M versus H were performed from 70 kOe to −70 kOe and from −70 kOe to 70 kOe starting from 300 K, then at 200 K, 100 K, 5 K, and 400 K; the temperature was changed under the applied field of 70 kOe. In other words, after finishing M versus H measurements at, for example, 300 K, the field was kept

at 70 kOe, and the temperature was changed to 200 K. A piece of an HP-$BiFe_{0.6}Mn_{0.4}O_3$ pellet (41.12 mg) was used in the magnetic measurements. This pellet was then transformed to AP-$BiFe_{0.6}Mn_{0.4}O_3$ (by annealing in a furnace in the air at AP at 773 K for 10 min as described above), and the same pellet was used in magnetic measurements.

Differential scanning calorimetry (DSC) curves of a powder sample of HP-$BiFe_{0.6}Mn_{0.4}O_3$ were recorded on a Mettler Toledo DSC1 STAR^e system between 297 K and 773 K in an open Al capsule with a heating/cooling rate of 10 K/min. Two DSC runs were performed to check the reproducibility. No DSC anomalies were observed. Laboratory and synchrotron XRPD data were taken, and magnetic properties were measured for the sample after this DSC experiment, and the transformation to AP-$BiFe_{0.6}Mn_{0.4}O_3$ was confirmed.

4. Conclusions

In conclusion, two modifications of the $BiFe_{0.6}Mn_{0.4}O_3$ perovskite were prepared: the HP modification was prepared by the direct high-pressure high-temperature method at 6 GPa, and the AP modification was prepared with a "conversion polymorphism" strategy. The transformation of the HP modification to the AP modification was studied in situ, and crystal structures of both modifications were investigated with synchrotron powder X-ray diffraction. The peculiar magnetic properties of HP-$BiFe_{0.6}Mn_{0.4}O_3$ and AP-$BiFe_{0.6}Mn_{0.4}O_3$ were investigated and have been reported herein.

Funding: This research received no external funding.

Data Availability Statement: The raw data supporting the conclusions of this article will be made available by the author on request.

Acknowledgments: Synchrotron radiation was used at the powder diffraction beamline BL02B2 at SPring-8 with permission from the Japan Synchrotron Radiation Research Institute (Proposal Number: 2021A1334). We thank S. Kobayashi for his help at BL02B2 of SPring-8. MANA was supported by the World Premier International Research Center Initiative (WPI), MEXT, Japan.

Conflicts of Interest: The author declares no conflict of interest.

References

1. Tokura, Y.; Seki, S.; Nagaosa, N. Multiferroics of spin origin. *Rep. Prog. Phys.* **2014**, *77*, 076501. [CrossRef] [PubMed]
2. Fiebig, M.; Lottermoser, T.; Meier, D.; Trassin, M. The evolution of multiferroics. *Nature Rev. Mater.* **2016**, *1*, 16046. [CrossRef]
3. Khomskii, D.I. Multiferroics: Different ways to combine magnetism and ferroelectricity. *J. Magn. Magn. Mater.* **2006**, *306*, 1–8. [CrossRef]
4. Khomskii, D. Classifying Multiferroics: Mechanisms and Effects. *Physics* **2009**, *2*, 20. [CrossRef]
5. Schmid, H. Multi-ferroic Magnetoelectrics. *Ferroelectrics* **1994**, *162*, 317–338. [CrossRef]
6. Catalan, G.; Scott, J.F. Physics and applications of bismuth ferrite. *Adv. Mater.* **2009**, *21*, 2463–2485. [CrossRef]
7. Wang, J.; Neaton, J.B.; Zheng, H.; Nagarajan, V.; Ogale, S.B.; Liu, B.; Viehland, D.; Vaithyanathan, V.; Schlom, D.G.; Waghmare, U.V.; et al. Epitaxial $BiFeO_3$ multiferroic thin film heterostructures. *Science* **2003**, *299*, 1719–1722. [CrossRef] [PubMed]
8. Bousquet, E.; Cano, A. Non-collinear magnetism in multiferroic perovskites. *J. Phys. Condens. Matter* **2016**, *28*, 123001. [CrossRef]
9. Zhang, R.Q.; Dong, H.F.; Wen, M.R.; Wu, F.G. Pressure-Induced Phase Diagram and Electronic Structure Evolves during the Insulator-Metal Transition of Bulk $BiFeO_3$. *Inorg. Chem.* **2023**, *62*, 16059–16067. [CrossRef]
10. Wu, Y.; Han, X.; Huang, H.J. Structural transformation pathways of multiferroic $BiFeO_3$ under high pressures. *J. Phys. Chem. C* **2018**, *122*, 6852–6857. [CrossRef]
11. Knee, C.S.; Tucker, M.G.; Manuel, P.; Cai, S.Z.; Bielecki, J.; Borjesson, L.; Eriksson, S.G. High pressure crystal and magnetic phase transitions in multiferroic $Bi_{0.9}La_{0.1}FeO_3$. *Chem. Mater.* **2014**, *26*, 1180–1186. [CrossRef]
12. Khomchenko, V.A.; Shvartsman, V.V.; Borisov, P.; Kleemann, W.; Kiselev, D.A.; Bdikin, I.K.; Vieira, J.M.; Kholkin, A.L. Effect of Gd substitution on the crystal structure and multiferroic properties of $BiFeO_3$. *Acta Mater.* **2009**, *57*, 5137–5145. [CrossRef]
13. Rusakov, D.A.; Abakumov, A.M.; Yamaura, K.; Belik, A.A.; Van Tendeloo, G.; Takayama-Muromachi, E. Structural evolution of the $BiFeO_3-LaFeO_3$ system. *Chem. Mater.* **2011**, *23*, 285–292. [CrossRef]
14. Troyanchuk, I.O.; Karpinsky, D.V.; Bushinsky, M.V.; Khomchenko, V.A.; Kakazei, G.N.; Araujo, J.P.; Tovar, M.; Sikolenko, V.; Efimov, V.; Kholkin, A.L. Isothermal structural transitions, magnetization and large piezoelectric response in $Bi_{1-x}La_xFeO_3$ perovskites. *Phys. Rev. B* **2011**, *83*, 054109. [CrossRef]
15. Karpinsky, D.V.; Troyanchuk, I.O.; Tovar, M.; Sikolenko, V.; Efimov, V.; Efimova, E.; Shur, V.Y.; Kholkin, A.L. Temperature and composition-induced structural transitions in $Bi_{1-x}La(Pr)_xFeO_3$ ceramics. *J. Am. Ceram. Soc.* **2014**, *97*, 2631–2638. [CrossRef]

16. Khomchenko, V.A.; Troyanchuk, I.O.; Tobbens, D.M.; Sikolenko, V.; Paixao, J.A. Composition- and temperature-driven structural transitions in $Bi_{1-x}Ca_xFeO_3$ multiferroics: A neutron diffraction study. *J. Phys. Condens. Matter* **2013**, *25*, 135902. [CrossRef]
17. Belik, A.A.; Abakumov, A.M.; Tsirlin, A.A.; Hadermann, J.; Kim, J.; Van Tendeloo, G.; Takayama-Muromachi, E. Structure and magnetic properties of $BiFe_{0.75}Mn_{0.25}O_3$ perovskite prepared at ambient and high pressure. *Chem. Mater.* **2011**, *23*, 4505–4514. [CrossRef]
18. Bhattacharjee, S.; Pandey, D. Stability of the various crystallographic phases of the multiferroic $(1-x)BiFeO_3-xPbTiO_3$ system as a function of composition and temperature. *J. Appl. Phys.* **2010**, *107*, 124112. [CrossRef]
19. Karpinsky, D.V.; Silibin, M.V.; Trukhanov, S.V.; Trukhanov, A.V.; Zhaludkevich, A.L.; Latushka, S.I.; Zhaludkevich, D.V.; Khomchenko, V.A.; Alikin, D.O.; Abramov, A.S.; et al. Peculiarities of the crystal structure evolution of $BiFeO_3$–$BaTiO_3$ ceramics across structural phase transitions. *Nanomaterials* **2020**, *10*, 801. [CrossRef]
20. Selbach, S.M.; Tybell, T.; Einarsrud, M.A.; Grande, T. Structure and properties of multiferroic oxygen hyperstoichiometric $BiFe_{1-x}Mn_xO_{3+\delta}$. *Chem. Mater.* **2009**, *21*, 5176–5186. [CrossRef]
21. Selbach, S.M.; Tybell, T.; Einarsrud, M.A.; Grande, T. High-temperature semiconducting cubic phase of $BiFe_{0.7}Mn_{0.3}O_{3+\delta}$. *Phys. Rev. B* **2009**, *79*, 214113. [CrossRef]
22. Belik, A.A. Polar and nonpolar phases of $BiMO_3$: A review. *J. Solid State Chem.* **2012**, *195*, 32–40. [CrossRef]
23. Khalyavin, D.D.; Salak, A.N.; Fertman, E.L.; Kotlyar, O.V.; Eardley, E.; Olekhnovich, N.M.; Pushkarev, A.V.; Radyush, Y.V.; Fedorchenko, A.V.; Desnenko, V.A.; et al. The phenomenon of conversion polymorphism in Bi-containing metastable perovskites. *Chem. Commun.* **2019**, *55*, 4683–4686. [CrossRef] [PubMed]
24. Belik, A.A. Origin of magnetization reversal and exchange bias phenomena in solid solutions of $BiFeO_3$–$BiMnO_3$: Intrinsic or extrinsic? *Inorg. Chem.* **2013**, *52*, 2015–2021. [CrossRef] [PubMed]
25. Mandal, P.; Sundaresan, A.; Rao, C.N.R.; Iyo, A.; Shirage, P.M.; Tanaka, Y.; Simon, C.; Pralong, V.; Lebedev, O.I.; Caignaert, V.; et al. Temperature-induced magnetization reversal in $BiFe_{0.5}Mn_{0.5}O_3$ synthesized at high pressure. *Phys. Rev. B* **2010**, *82*, 100416. [CrossRef]
26. Levin, I.; Tucker, M.G.; Wu, H.; Provenzano, V.; Dennis, C.L.; Karimi, S.; Comyn, T.; Stevenson, T.; Smith, R.I.; Reaney, I.M. Displacive phase transitions and magnetic structures in Nd-substituted $BiFeO_3$. *Chem. Mater.* **2011**, *23*, 2166–2175. [CrossRef]
27. Corker, D.L.; Glazer, A.M.; Dec, J.; Roleder, K.; Whatmore, R.W. A re-investigation of the crystal structure of the perovskite $PbZrO_3$ by X-ray and neutron diffraction. *Acta Crystallogr. Sect. B Struct. Sci.* **1997**, *53*, 135–142. [CrossRef]
28. Teslic, S.; Egami, T. Atomic structure of $PbZrO_3$ determined by pulsed neutron diffraction. *Acta Crystallogr. Sect. B Struct. Sci.* **1998**, *54*, 750–765. [CrossRef]
29. Khomchenko, V.A.; Troyanchuk, I.O.; Maria, T.M.R.; Karpinsky, D.V.; Das, S.; Amaral, V.S.; Paixao, J.A. Mn doping-induced structural and magnetic transformations in the antiferroelectric phase of the $Bi_{1-x}Nd_xFeO_3$ perovskites. *J. Appl. Phys.* **2012**, *112*, 064105. [CrossRef]
30. Karpinsky, D.V.; Silibin, M.V.; Latushka, S.I.; Zhaludkevich, D.V.; Sikolenko, V.V.; Al-Ghamdi, H.; Almuqrin, A.H.; Sayyed, M.I.; Belik, A.A. Structural and magnetic phase transitions in $BiFe_{1-x}Mn_xO_3$ solid solution driven by temperature. *Nanomaterials* **2022**, *12*, 1565. [CrossRef]
31. Karpinsky, D.V.; Silibin, M.V.; Latushka, S.I.; Zhaludkevich, D.V.; Sikolenko, V.V.; Svetogorov, R.; Sayyed, M.I.; Almousa, N.; Trukhanov, A.; Trukhanov, S.; et al. Temperature-driven transformation of the crystal and magnetic structures of $BiFe_{0.7}Mn_{0.3}O_3$ ceramics. *Nanomaterials* **2022**, *12*, 2813. [CrossRef] [PubMed]
32. Manna, P.K.; Yusuf, S.M.; Shukla, R.; Tyagi, A.K. Exchange bias in $BiFe_{0.8}Mn_{0.2}O_3$ nanoparticles with an antiferromagnetic core and a diluted antiferromagnetic shell. *Phys. Rev. B* **2011**, *83*, 184412. [CrossRef]
33. Fertman, E.L.; Fedorchenko, A.V.; Desnenko, V.A.; Shvartsman, V.V.; Lupascu, D.C.; Salamon, S.; Wende, H.; Vaisburd, A.I.; Stanulis, A.; Ramanauskas, R.; et al. Exchange bias effect in bulk multiferroic $BiFe_{0.5}Sc_{0.5}O_3$. *AIP Adv.* **2020**, *10*, 045102. [CrossRef]
34. Kawaguchi, S.; Takemoto, M.; Osaka, K.; Nishibori, E.; Moriyoshi, C.; Kubota, Y.; Kuroiwa, Y.; Sugimoto, K. High-throughput powder diffraction measurement system consisting of multiple MYTHEN detectors at beamline BL02B2 of SPring-8. *Rev. Sci. Instrum.* **2017**, *88*, 085111. [CrossRef] [PubMed]
35. Izumi, F.; Ikeda, T. A Rietveld-analysis program RIETAN-98 and its applications to zeolites. *Mater. Sci. Forum* **2000**, *321–324*, 198–205. [CrossRef]